Electronic Supplementary Material (ESI) for Nanoscale.

Supporting Information

Single-trigger dual-responsive nanoparticles for controllable and sequential prodrug activation

Neil M. Robertson[†], Yang Yang[†], Irfan Khan[†], Vincent E. LaMantia[†], Maksim Royzen[†, ‡, *], and Mehmet V. Yigit [†, ‡, *]

† Department of Chemistry,
University at Albany, State University of New York,
1400 Washington Avenue, Albany, New York 12222, United States.

‡ The RNA Institute,
University at Albany, State University of New York,
1400 Washington Avenue, Albany, New York 12222, United States.

*Correspondence:

Tel: (1) 518-442-3002

myigit@albany.edu

Tel: (1) 518-437-4463

mroyzen@albany.edu

Supporting Figures

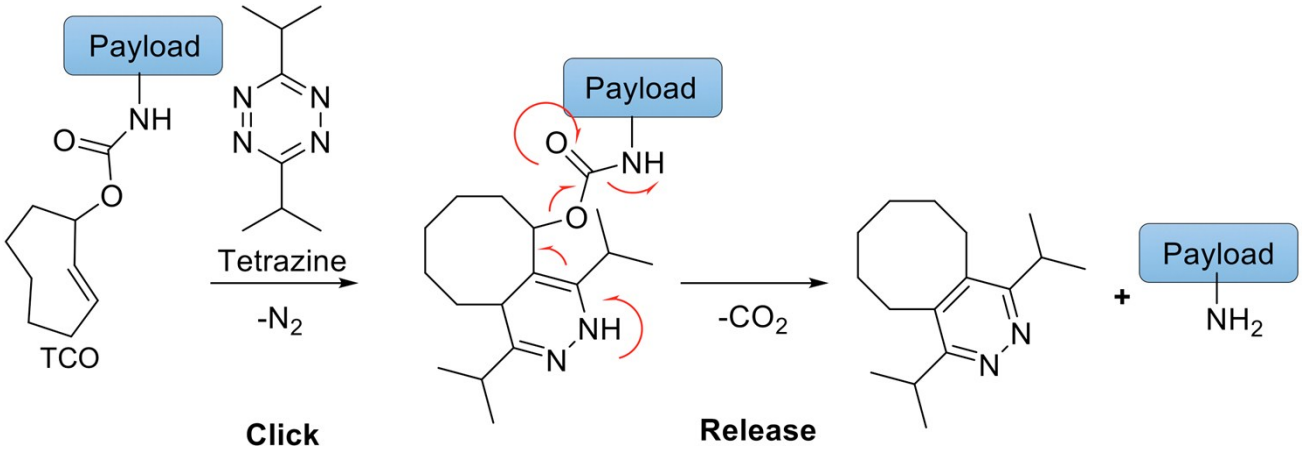

Figure S1: Bioorthogonal chemistry for release and activation of functional payloads through the *'click-to-release'* mechanism.

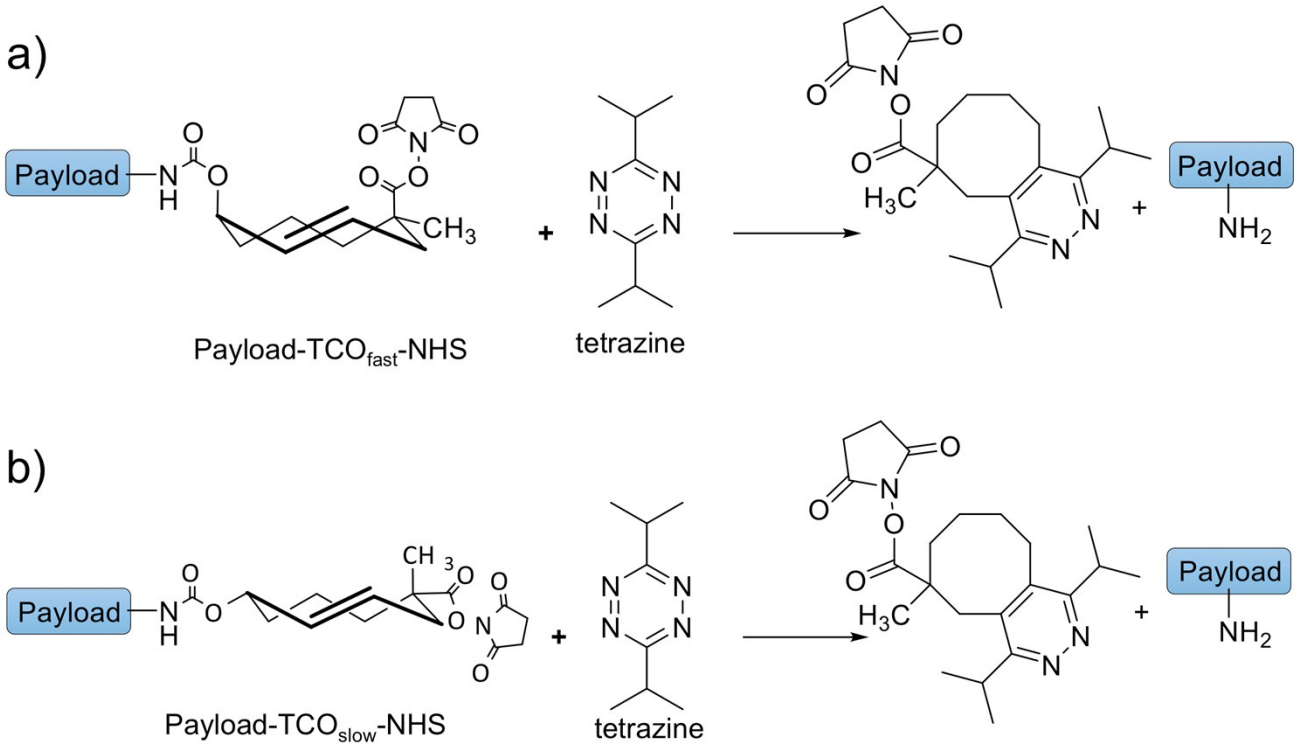

Figure S2: *Click-to-release* bioorthogonal chemistry for activation of functional payloads through **a)** fast and **b)** slow acting TCO-linkers.

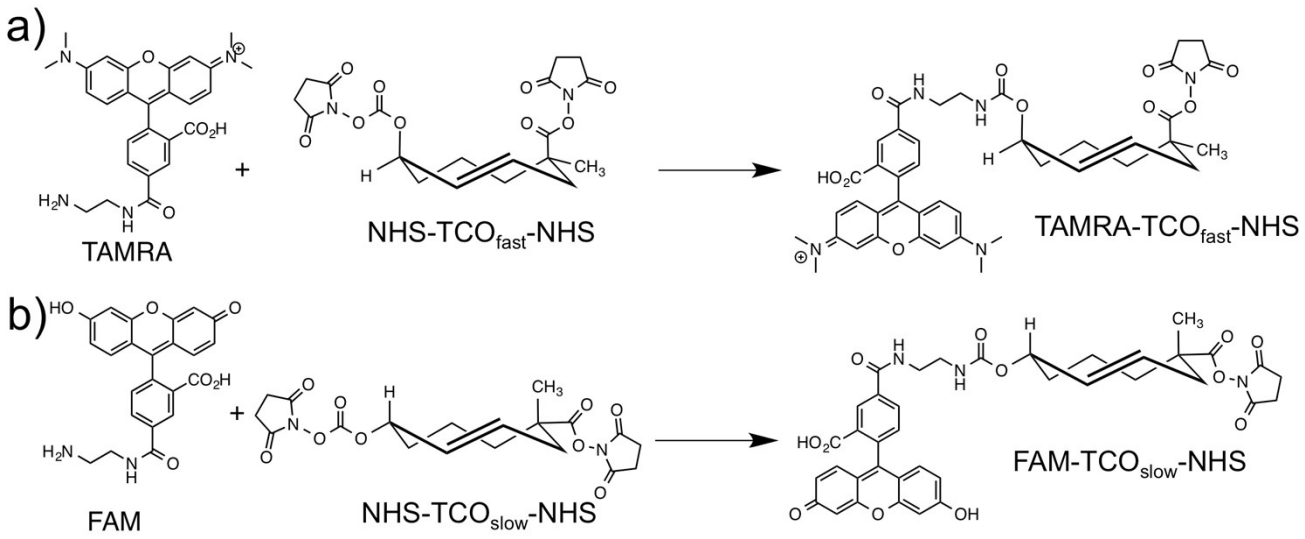

Figure S3: Functionalization of **a)** TAMRA with fast acting TCO linker (NHS-TCO$_{fast}$-NHS) and **b)** FAM with slow acting TCO linker (NHS-TCO$_{slow}$-NHS). The NHS in the allylic position is more reactive to amines, enabling the synthesis of the chemically illustrated products of TAMRA-TCO$_{fast}$-NHS and FAM-TCO$_{slow}$-NHS.

a)

Nanoparticles	Size (%PD)	Zeta Potential (mV)
MNP	12.34 (12.7)	22.2 ± 2.6
MNP-D_f	10.2 (0)	30.0 ± 1.1
MNP-P_f	13.5 (0)	41.9 ± 2.1
MNP-D_fP_f	10.2 (0)	28.9 ± 1.3
MNP-D_sP_f	12.4 (12.5)	29.3 ± 0.5

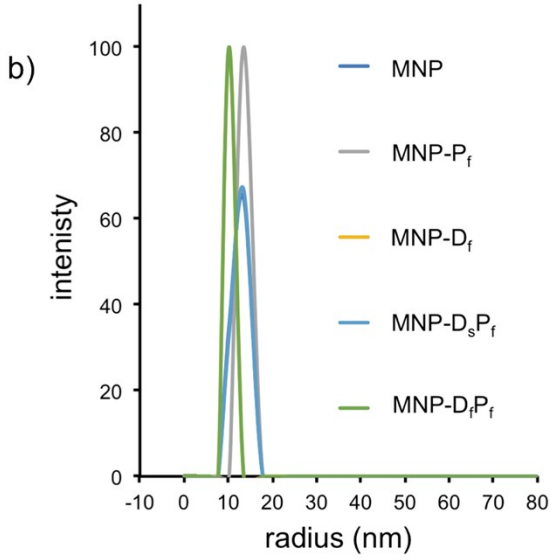

Figure S4: a) Table showing the zeta potential and size of the MNPs. b) Hydrodynamic radii of the nanoparticle constructs.

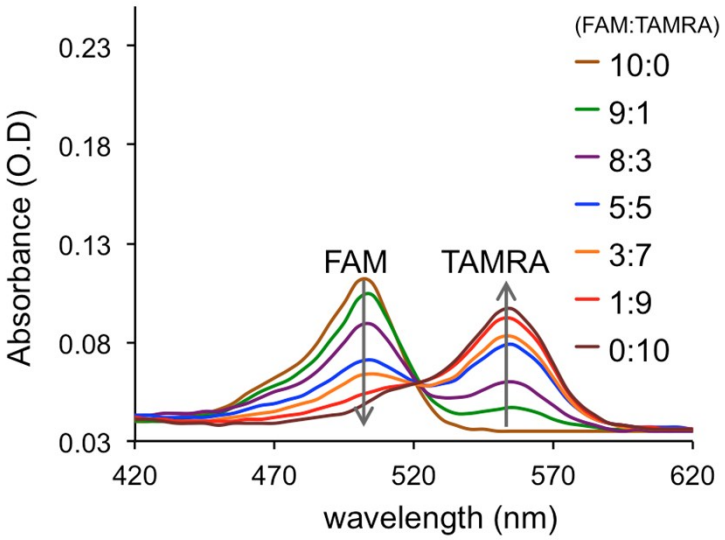

Figure S5: Fluorescence of ratiometrically prepared free TAMRA-TCO_{fast}-NHS and FAM-TCO_{slow}-NHS**.**

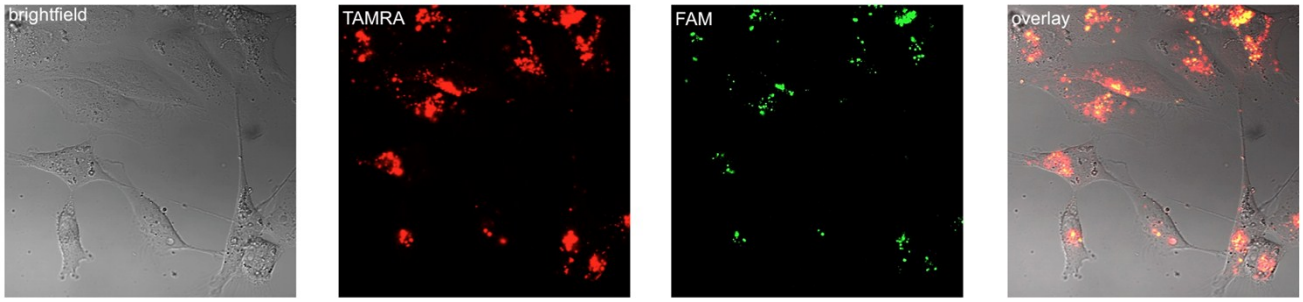

Figure S6: Additional confocal microscopy demonstrating that the **MNPs**-F_sT_f are efficiently taken up, which can be monitored by TAMRA and FAM emission channels.

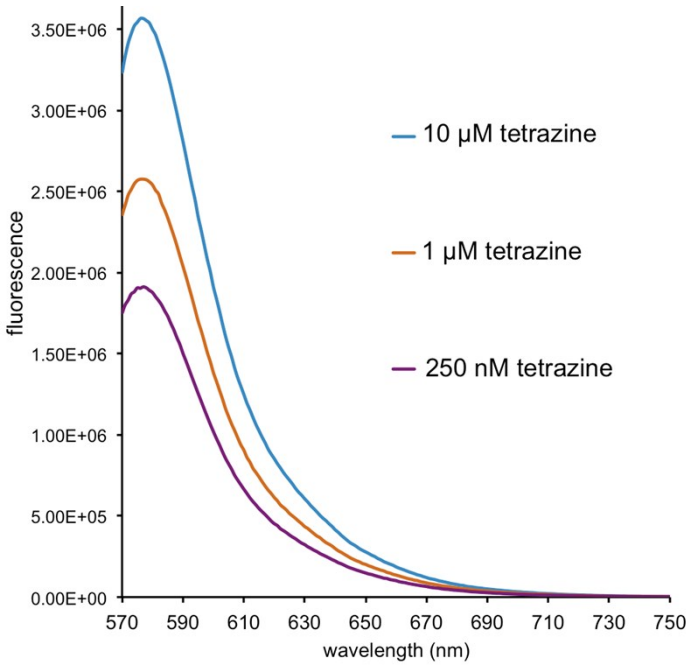

Figure S7: Release of the TAMRA payload attached on the **MNP**-F_sT_f surface in response to different concentrations of tetrazine.

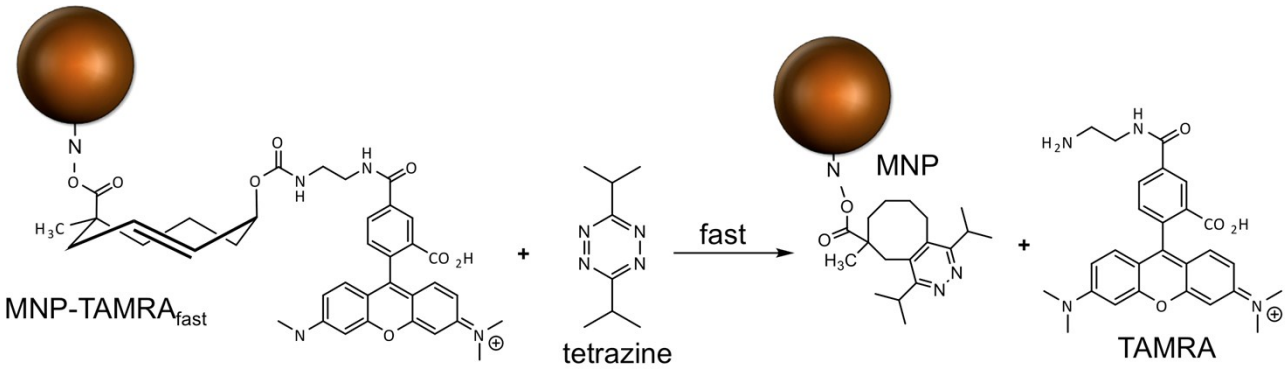

Figure S8: Release of the TAMRA payload attached on the MNP surface in response to tetrazine through the fast *click-to-release* mechanism.

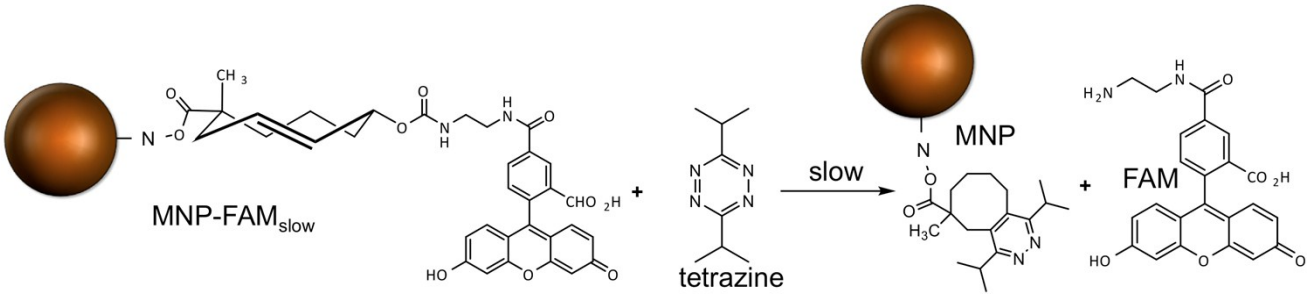

Figure S9: Release of the FAM payload attached on the MNP surface in response to tetrazine through the slow *click-to-release* mechanism.

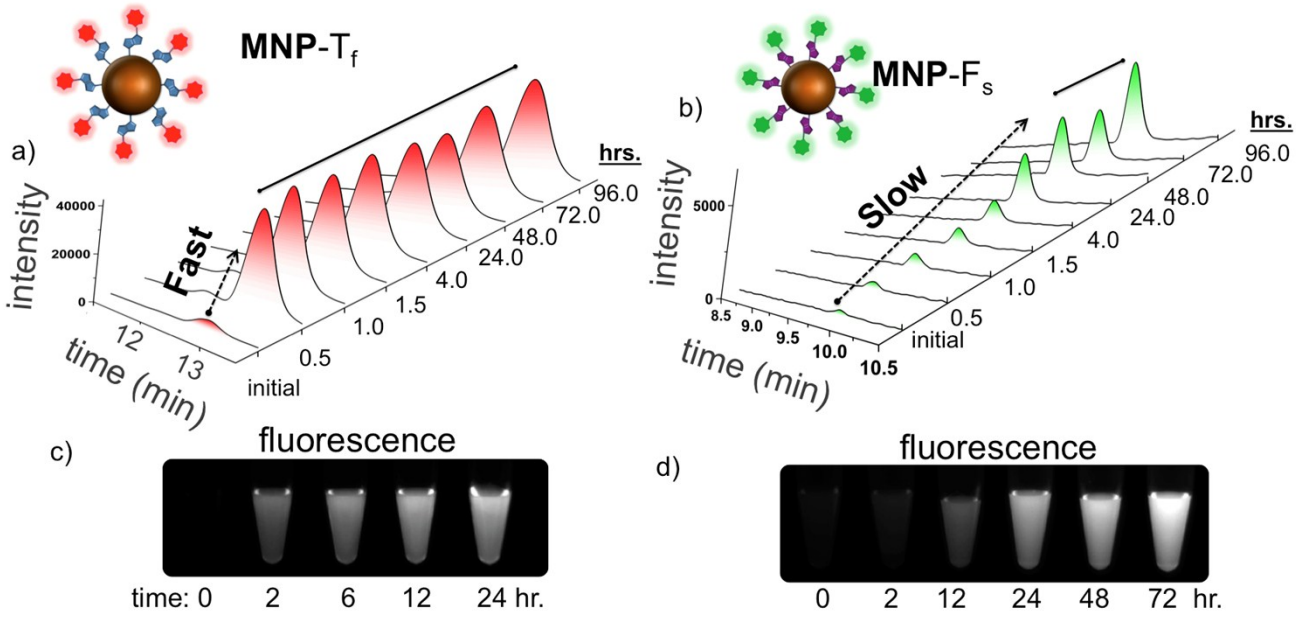

Figure S10: Controlled release of the MNP-T_f and MNP-F_s with a single dose of tetrazine. a) TAMRA payload attached via the TCO_{fast} linker is observed to release by 30 minutes, with no change in intensity seen through 96 hours. In contrast, the b) FAM payload attached to the TCO_{slow} linker was observed to have insignificant release prior to 24 hours and no change in intensity after 48 hours. Initial measurements with no tetrazine addition were used as controls. c-d) A separate study showing the qualitative fluorescent images of the supernatants recovered after treatment of c) **MNP-T_f and** d) **MNP-F_s** with tetrazine. TAMRA release is observed to be faster than FAM release.

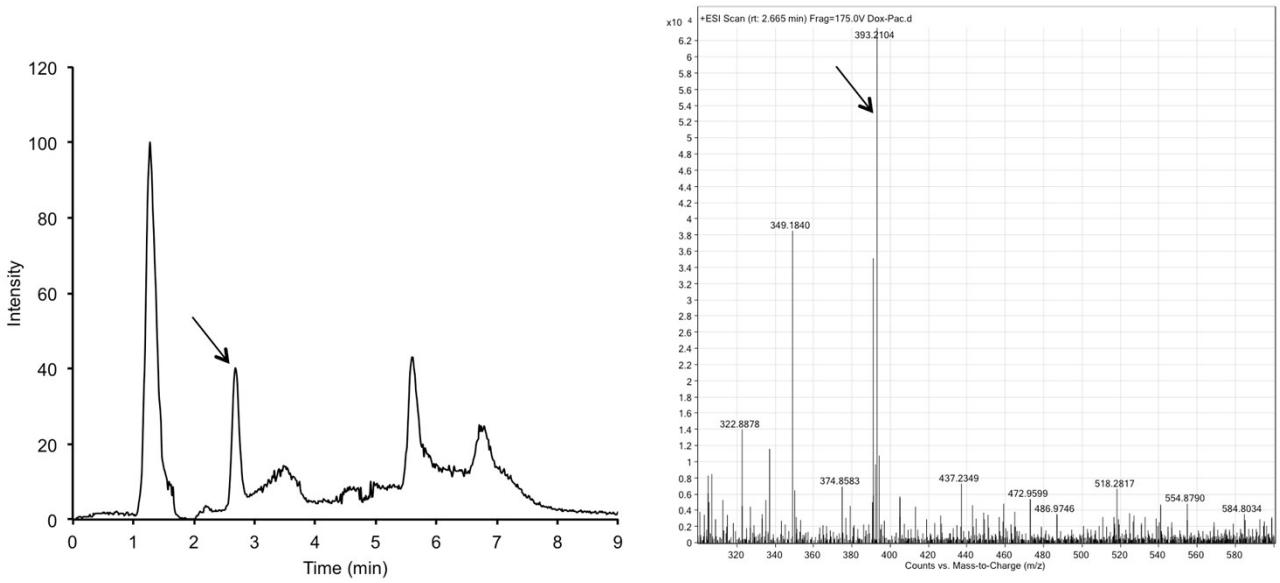

Figure S11: Liquid chromatography-mass spectrometry (LC-MS) data of the **MNP-P$_f$** 30 min after treatment with 1 μM tetrazine. The left spectrum is showing extracted mass of 393 from the total ion current. The arrow is pointing to the peak corresponding to the released drug. The observed mass spectrum is shown on the right, [M+H]+ (calc'd for $C_{23}H_{29}N_4O_2$)= 393.2291. Other peaks observed on the extracted mass chromatogram correspond to buffer, polydextran fragments and inorganic materials comprising the MNPs.

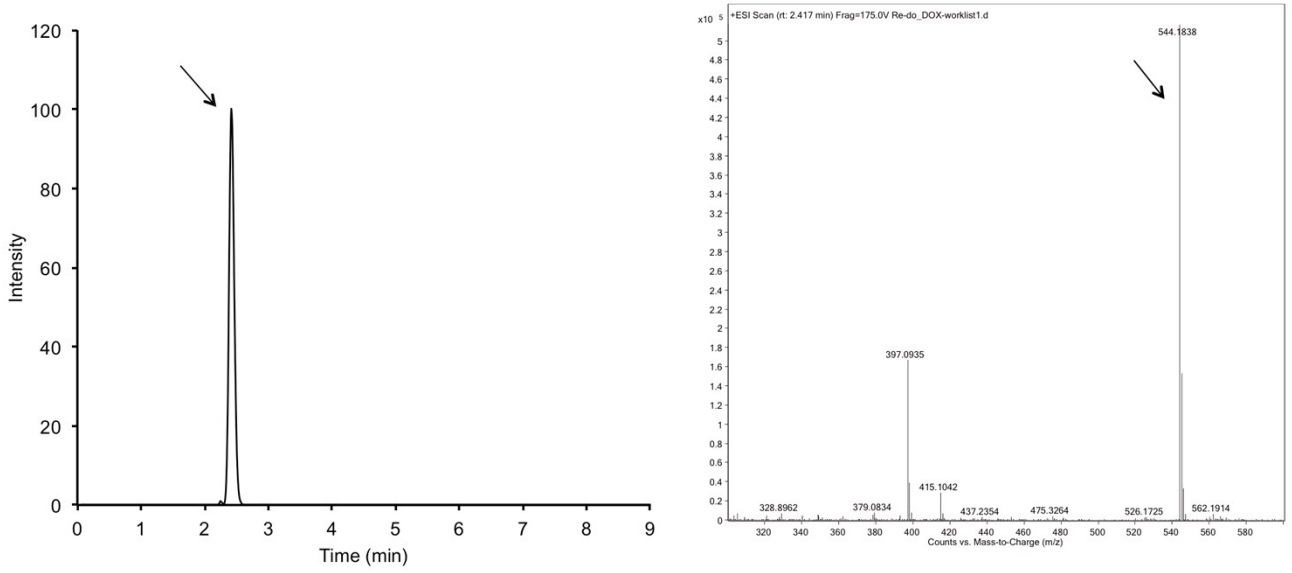

Figure S12: Liquid chromatography-mass spectrometry (LC-MS) data of the MNP-D_f 30 min after treatment with 1 μM tetrazine. The left spectrum is showing extracted mass of 544 from the total ion current. The arrow is pointing to the peak corresponding to the released drug. The observed mass spectrum is shown on the right, [M+H]+ (calc'd for $C_{27}H_{30}NO_{11}$)= 544.1819. Other peaks observed on the extracted mass chromatogram correspond to buffer, polydextran fragments and inorganic materials comprising the MNPs.

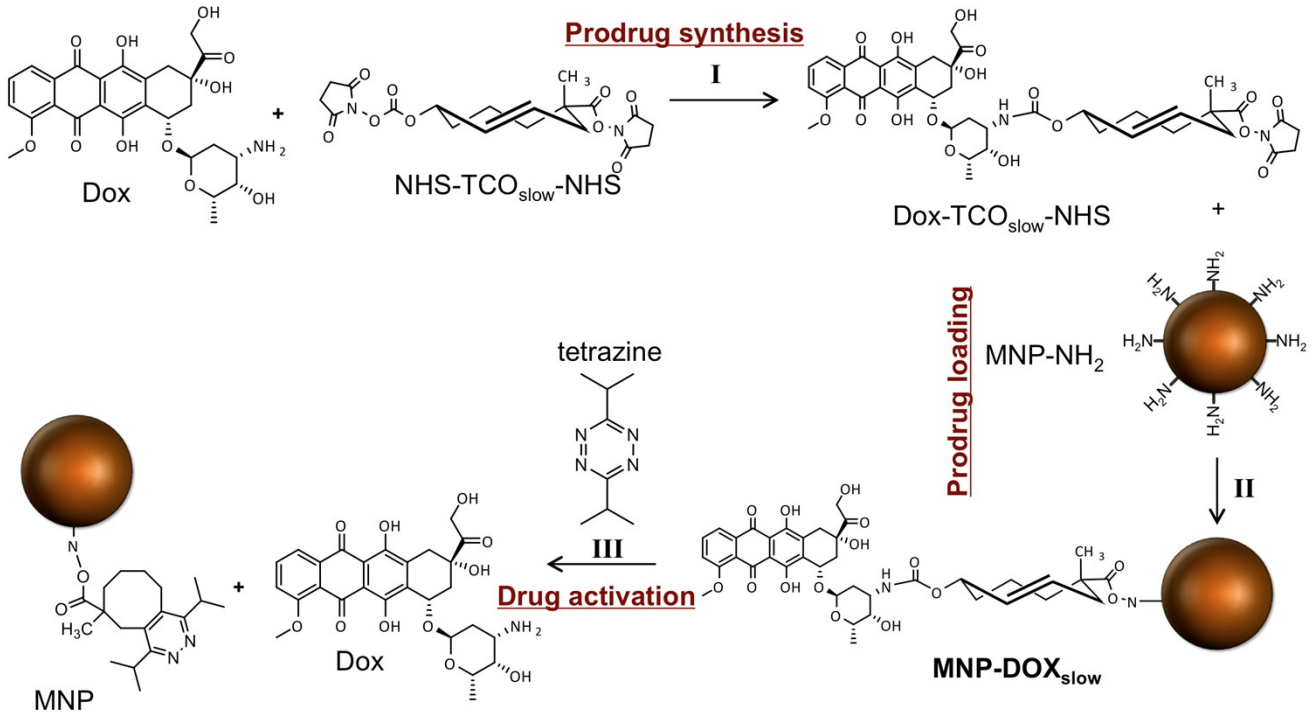

Figure S13: *Step I*. Synthesis of doxorubicin-TCO$_{slow}$-NHS molecule using the slow acting TCO-linker. *Step II*. Attachment of doxorubicin prodrug on the MNP surface. *Step III*. Release, therefore activation, of doxorubicin in response to tetrazine.

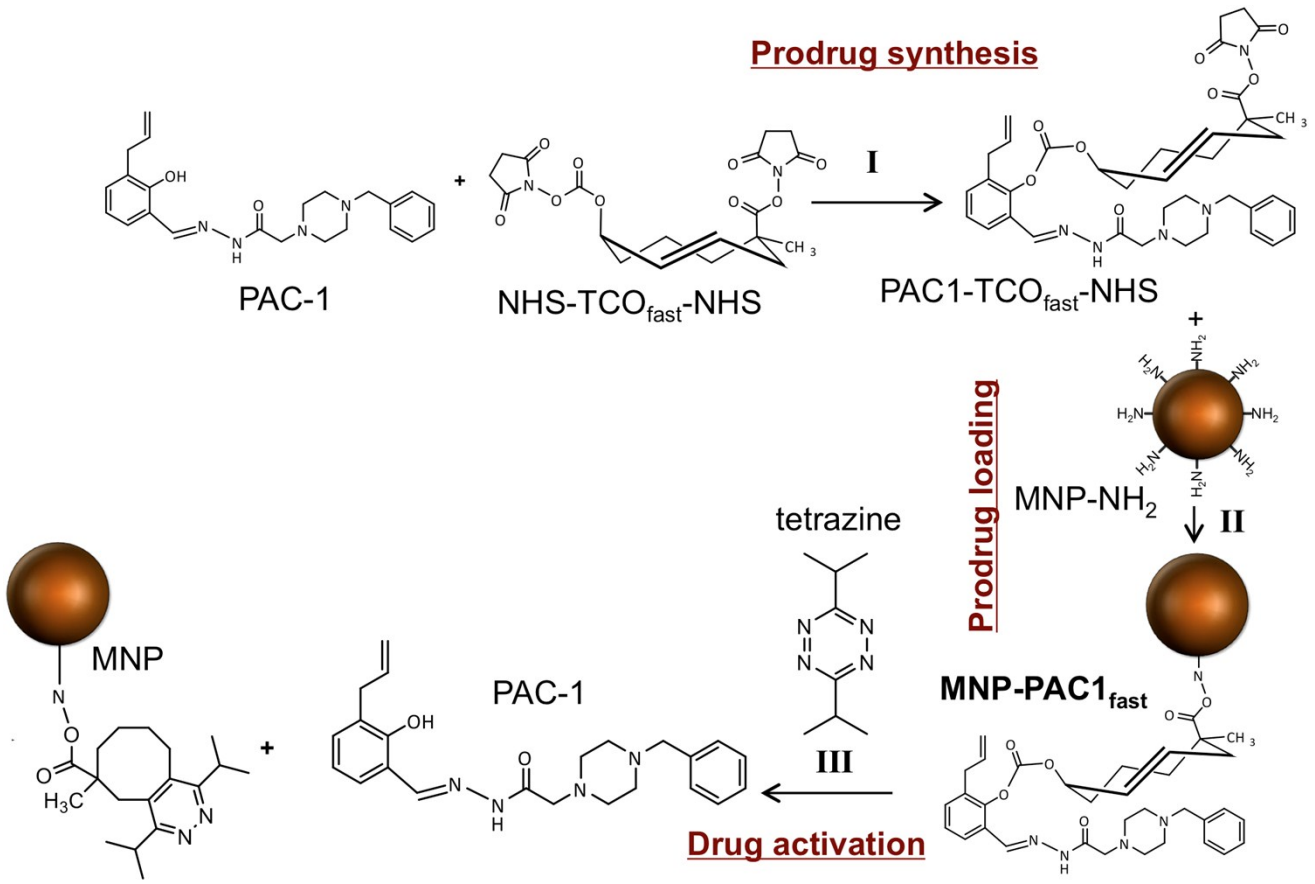

Figure S14: *Step I*. Synthesis of PAC1-TCO$_{fast}$-NHS molecule using the fast acting TCO-linker. *Step II*. Attachment of PAC1 prodrug on the MNP surface. *Step III*. Release, therefore activation, of PAC1 in response to tetrazine.

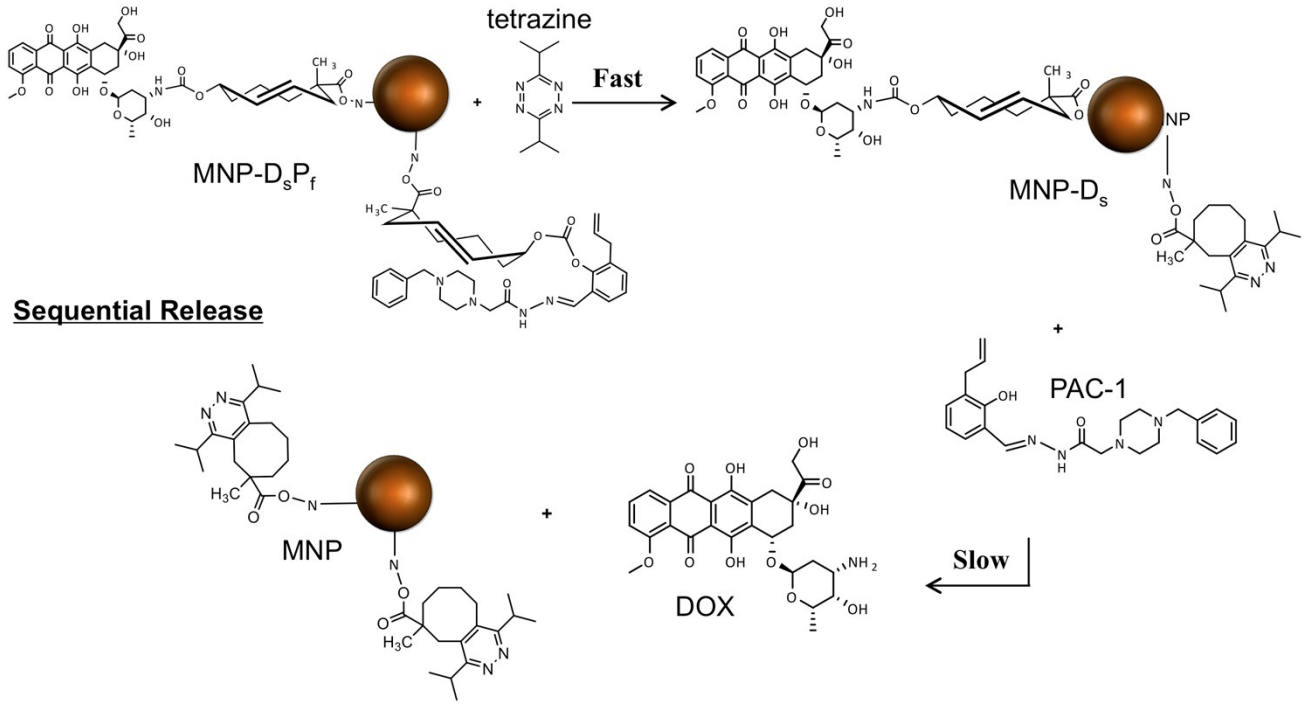

Figure S15: Time-staggered activation of PAC-1 and DOX prodrugs loaded on the **MNP**-D_sP_f nanodrug in response to a single administration of tetrazine.

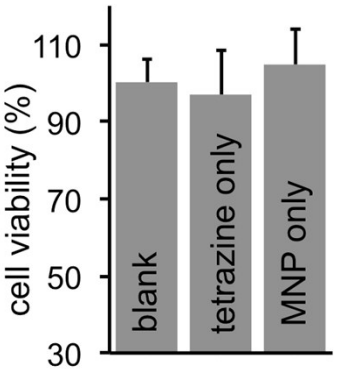

Figure S16: Cell viability assay showing that tetrazine or MNP only does not display any cellular toxicity.

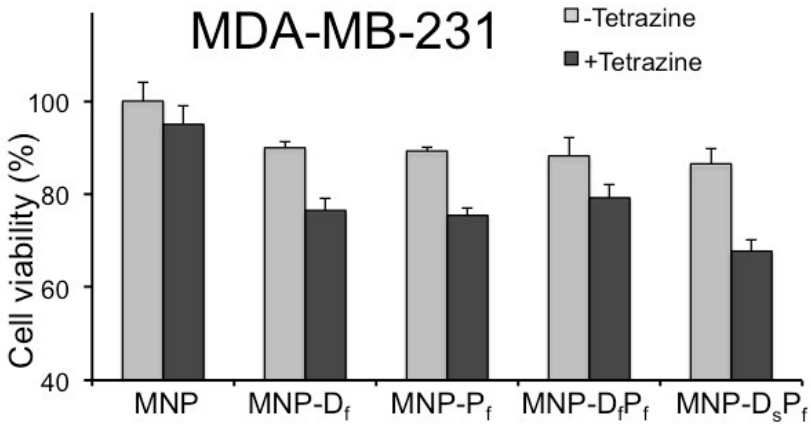

Figure S17: Cell viability assays performed with MDA-MB-231. Administration of MNP constructs (**MNP**, **MNP**-D_f, **MNP**-P_f, **MNP**-D_fP_f and **MNP**-D_sP_f) with and without tetrazine post-administration.

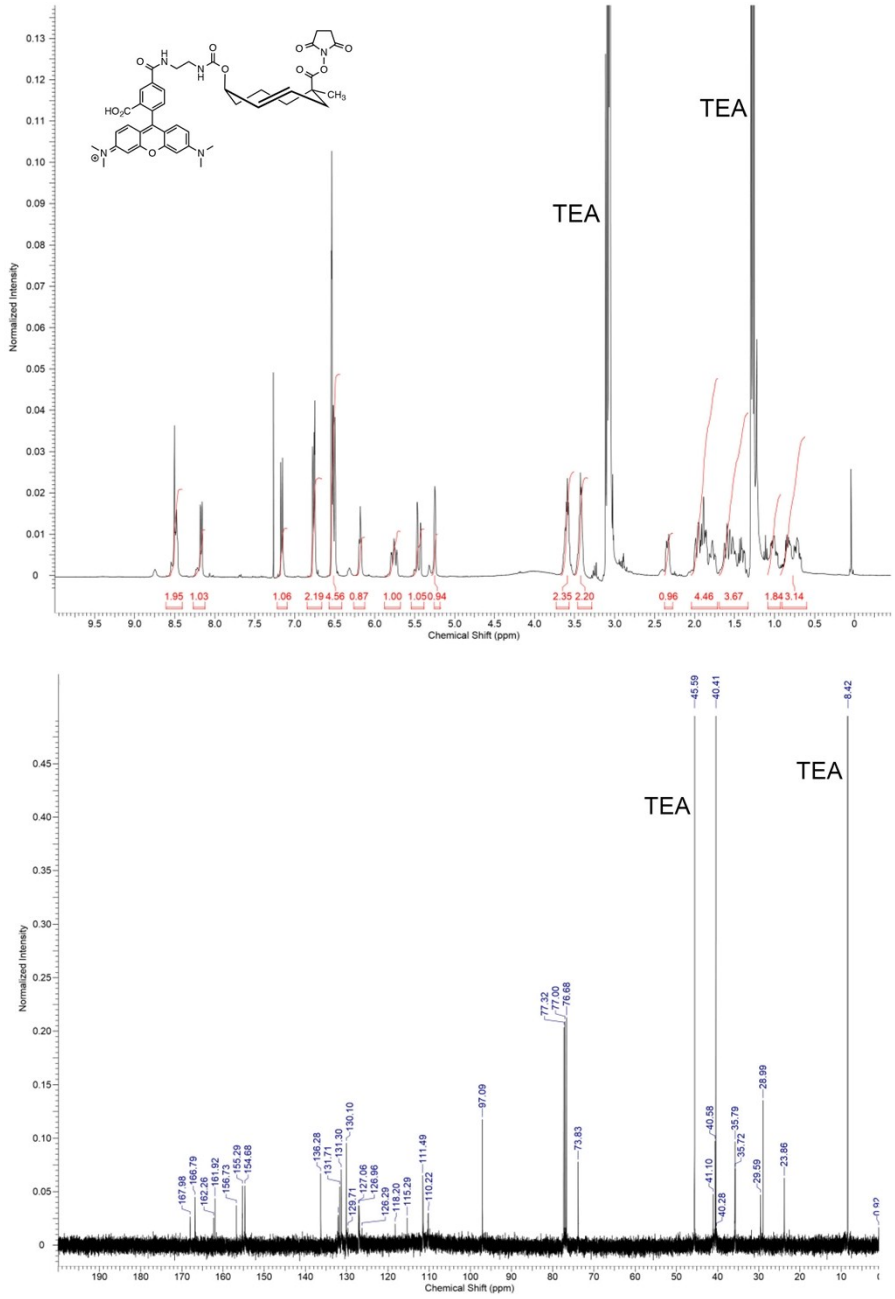

Figure S18: NMR and HRMS results of TAMRA-TCO$_{fast}$-NHS

^{1}H NMR ($CDCl_3$, 400 MHz) δ: 8.50-8.48 (m, 2H), 8.17 (d, *J* = 8.2 Hz, 1H), 7.16 (d, *J* = 8.2 Hz, 1H), 6.77-6.75 (m, 2H), 6.54-6.50 (m, 5H), 6.18 (t, *J* = 5.4 Hz, 1H), 5.79-5.72 (m, 1H), 5.47-5.43 (m, 1H), 5.25 (s, 1H), 3.62-3.58 (m, 2H), 3.43-3.42 (m, 2H), 2.35-2.32 (m, 1H), 1.99-1.75 (m, 4H), 1.62-1.38 (m, 4H), 1.31 (s, 3H), 1.05-1.00 (m, 2H), 0.86-0.69 (m, 3H).

^{13}C{^{1}H} NMR ($CDCl_3$, 100 MHz) δ: 167.98, 166.79, 162.26, 161.92, 156.73, 155.29, 154.68, 136.28, 132.06, 131.71, 131.30, 130.10, 127.06, 126.96, 118.20, 115.29, 111.49, 110.22, 97.09, 73.83, 41.10, 40.58, 40.41, 35.79, 35.72, 29.59, 26.99, 23.86.
HRMS (ESI-MS) *m/z*: calcd. for $C_{42}H_{45}N_5NaO_{10}$ $[M+Na]^+$ 802.3059; found 802.2893. yield = 50 mg (58 %).

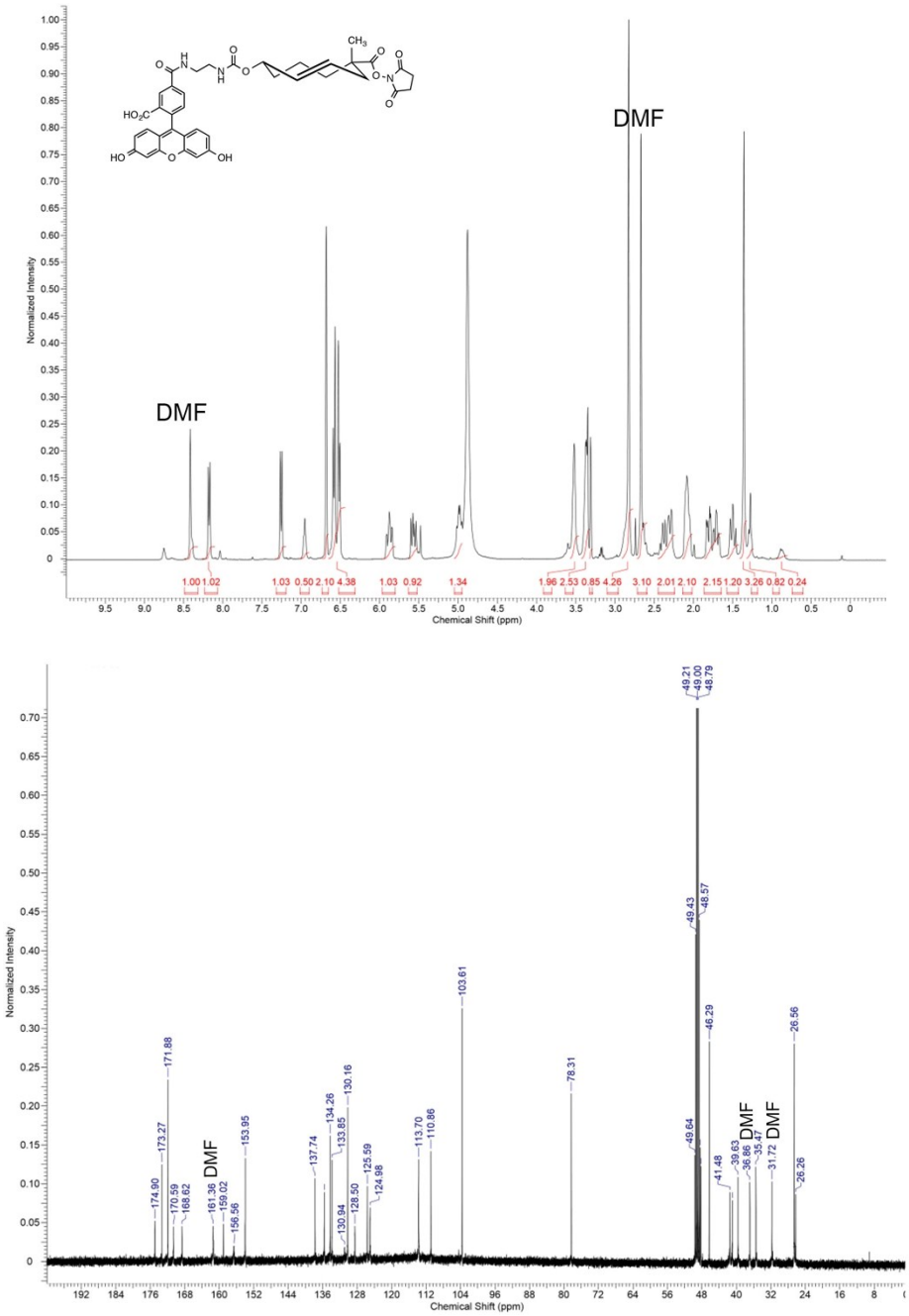

Figure S19: NMR and HRMS results of FAM-TCO$_{slow}$-NHS

^{1}H NMR (CD$_3$OD, 400 MHz) δ: 8.18 (d, *J* = 8.2 Hz, 1H), 7.26 (d, *J* = 8.1 Hz, 1H), 6.96 (br s, 1H), 6.68 (s, 2H), 6.55 (q, J_1 = 24.6 Hz, J_2 = 8.2 Hz, 4H), 5.88 (t, *J* = 12.2 Hz, 1H), 5.60-5.54 (m, 1H), 5.02-4.95 (m, 1H), 3.52 (br s, 2H), 3.37-3.35 (m, 2H), 2.42-2.28 (m, 2H), 2.08 (br s, 2H), 1.83-1.69 (m, 2H), 1.50 (t, *J* = 13.6 Hz, 1H), 1.35 (s, 3H), 1.28 (s, 1H).

^{13}C{^{1}H} NMR (CD$_3$OD, 100 MHz) δ: 174.90, 173.27, 171.88, 170.59, 166.62, 159.02, 156.56, 153.95, 137.74, 135.61, 134.26, 133.85, 130.94, 130.16, 128.50, 125.59, 124.98, 113.70, 110.86, 103.61, 78.31, 46.29, 41.48, 40.94, 39.63, 35.47, 26.56, 26.26.

HRMS (ESI-MS) *m/z*: calcd. for $C_{38}H_{36}N_3O_{12}$ $[M+H]^+$ 726.2299; found 726.2305. yield = 65 mg (54 %).

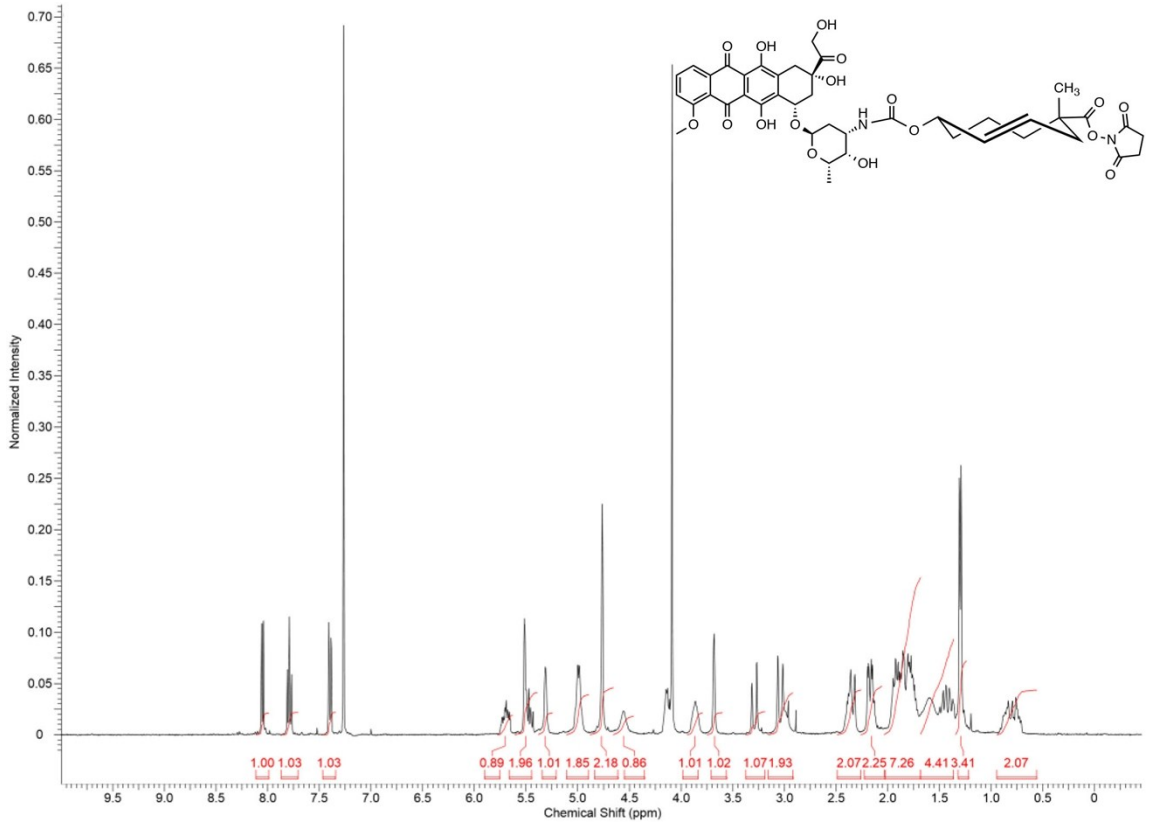

Figure S20: NMR and HRMS results of DOX-TCO$_{slow}$-NHS

^{1}H NMR ($CDCl_3$, 400 MHz) δ: 8.05 (d, *J* = 8.2 Hz, 1H), 7.79 (t, *J* = 8.2 Hz, 1H), 7.40 (d, *J* = 8.2 Hz, 1H), 5.73-5.66 (m, 1H), 5.52-5.44 (m, 2H), 5.31 (s, 1H), 5.0 (s, 2H), 4.76 (s, 2H), 4.56 (br s, 1H), 3.86 (br s, 1H), 3.68 (s, 1H), 3.31-3.27 (m, 1H), 3.06-2.96 (m, 2H), 2.39-2.32 (m, 2H), 2.19-2.13 (m, 2H), 1.95-1.73 (m, 7H), 1.60-1.40 (m, 4H), 1.30 (d, *J* = 6.8 Hz, 3H), 0.86-0.73 (m, 2H).

HRMS (ESI-MS) *m/z*: calcd. for $C_{42}H_{47}N_2O_{17}$ $[M+H]^+$ 851.8350; found 851.8229. yield = 77 mg (60 %).

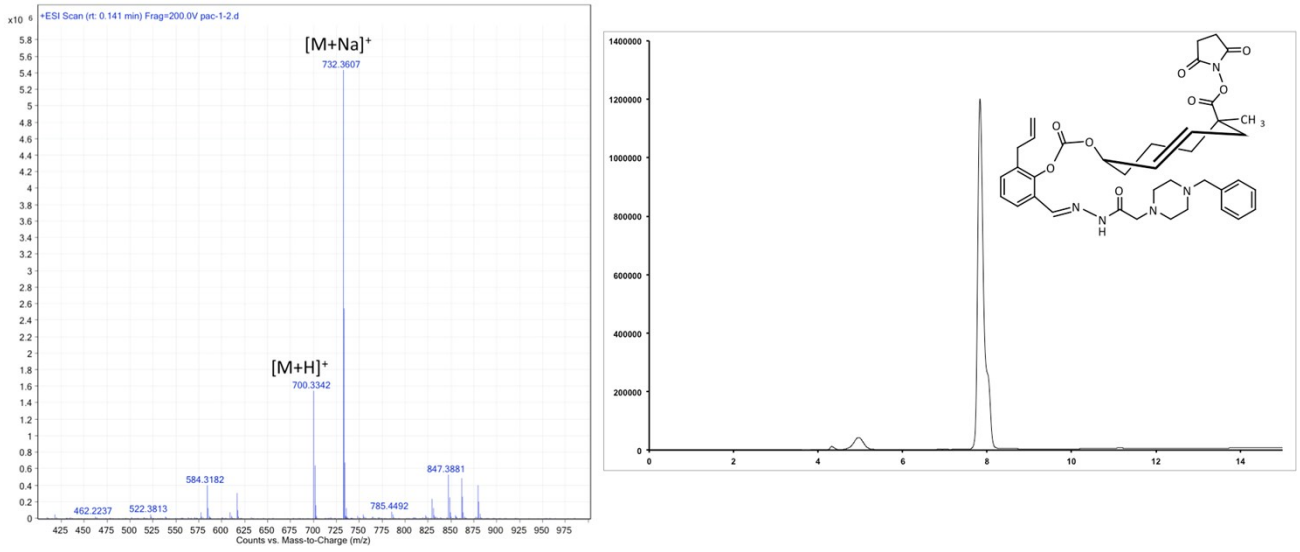

Figure S21: HRMS and HPLC results of PAC1-TCO$_{fast}$-NHS

HRMS (ESI-MS) *m/z*: calcd. for $C_{38}H_{46}N_5O_8$ $[M+H]^+$ 700.3346; found 700.3342. yield = 5 mg (3%).